Structure of a hard-sphere fluid near a rough surface: A density-functional approach

D. Henderson,[1] S. Sokołowski,[1,2] and D. Wasan[3]

[1]*Department of Chemistry and Biochemistry, Brigham Young University, Provo, Utah 84602*
[2]*Department for the Modelling of Physico-Chemical Processes, Faculty of Chemistry, Maria Curie Skłodowska University, 20031 Lublin, Poland*
[3]*Department of Chemical Engineering, Illinois Institute of Technology, Chicago, Illinois 60616*

The density-functional theory of Evans [in *Fundamentals of Inhomogeneous Fluids*, edited by D. Henderson (Dekker, New York, 1992)] and Tarazona [Phys. Rev. A **31**, 2672 (1985)] is used to study an inhomogeneous fluid near a rough surface or pore composed of grooves consisting of a periodic array of saw-toothed wedges. This involves a two-dimensional formulation of this approach, in contrast to the one-dimensional formulations that generally have been used previously. The agreement with the simulations of Schoen and Dietrich [Phys. Rev. E **56**, 499 (1997)] is good. [S1063-651X(98)09305-2]

I. INTRODUCTION

In recent years significant progress has been made in understanding fluid behavior in pores of different geometry [1–4]. In the majority of the theoretical studies, the substrate walls have been modeled by potentials that vary only in the direction perpendicular to the surface and are translationally invariant in lateral directions. Obviously, even for perfect crystals this is a simplification because of the atomic corrugation of the substrate [5]. Moreover, real surfaces are usually rough, so the fluid is exposed to a geometrically heterogeneous wall.

The effects of geometrical heterogeneity on the adsorption of fluids have been studied experimentally and theoretically [6–19]. Although most theoretical methods that have been used are coarse-gained approaches that laterally average the surface nonuniformity over the local height variation of the substrate [10–13], some studies based on the weighted local density theory [3] have also been undertaken [16–19]. However, our understanding of the microscopic structure of a fluid that fills the grooves and covers the tips of a geometrically heterogeneous substrate is far from being satisfactory.

Among the common techniques in liquid state theory [20], density-functional theories [3] have been shown to be both computationally simple and reliable for the description of simple liquids in an inhomogeneous phase. In this case, the most successful density-functional theories are those that involve a coarse-gained average density [3]. In a recently published paper, Schoen and Dietrich [21] have analyzed a hard-sphere fluid exposed to a periodic array of wedges by using the grand canonical ensemble Monte Carlo (GCEMC) simulation technique. In their model, the attractive forces between the fluid particles and the substrate are absent; thus the results obtained illustrate the purely entropic effects of the spatial confinement on the fluid structure. It is interesting to test the predictions of a version of the density-functional theory against the Schoen-Dietrich data. The principal aim of our work is thus to perform such a test and, if successful, to justify the application of this approach to more complicated geometries and interactions. Our description is based on the equations developed from the Evans-Tarazona version of density-functional theory [3,22].

II. THEORY

The model that we use is identical to that studied by Schoen and Dietrich; however, we employ a slightly different system of coordinates. The sketch of the system is given in Fig. 1. The unit cell consists of two oppositely placed hard wedges of dihedral angle γ in the OXZ plane. The corner of the wedge is at $x=0$ and two tips are at $x=s_x/2$ and $-s_x/2$. The lower and upper tips are separated by the distance s_z. The system is periodically extended in the x direction and is infinite in the y direction (perpendicular to the figure plane). The fluid particles interact via the hard-sphere potential.

$$u(r)=\begin{cases} 0, & r<\sigma \\ \infty, & r>\sigma. \end{cases} \tag{1}$$

If we consider only one-fourth of the cell shown in Fig. 1, defined by $0<x<s_x/2$ and $0<z<s_z/2+s_x/2\tan(\gamma/2)$, then the substrate-fluid potential is given by
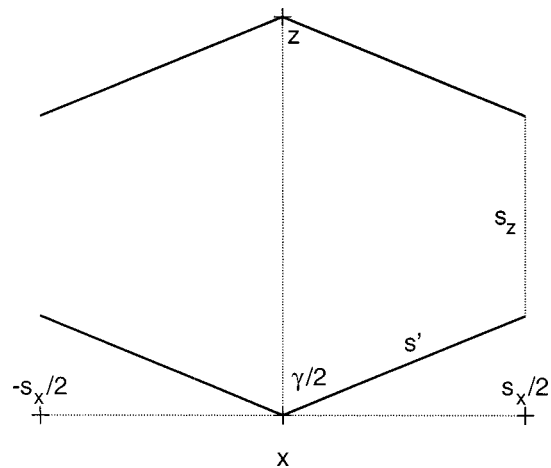
FIG. 1. Side view of the unit cell of the system consisting of two opposite hard wedges of side length s' and dihedral angle γ in the OXZ plane. The corner of the lower wedge is located at $x=0$ and $z=0$ and two tips at $x=-s_x/2$ and $s_x/2$ are separated by a distance s_z. The system is periodically extended in the x direction.
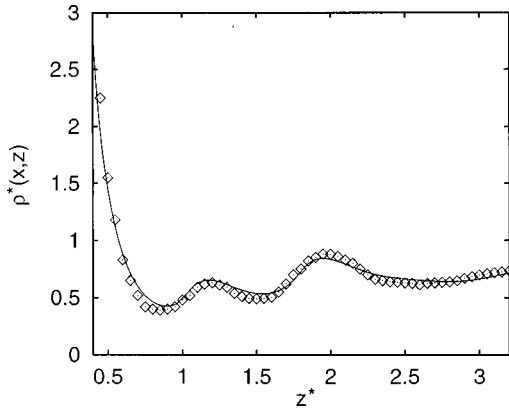
FIG. 2. Cut through the density distribution $\rho(x,z)$ by the plane $x=0.36$ as a function of $z^*=z/\sigma$ for $\gamma=\pi/2$. The solid line denotes the density-functional result, whereas points are the GCEMC data [21]. The calculations have been performed at $\rho_b^*=0.7016$.

$$v(z,x)=\begin{cases} 0, & z>x/\tan(\gamma/2) \\ \infty, & z<x/\tan(\gamma/2). \end{cases} \quad (2)$$

The fluid is inhomogeneous in both the z and x directions; the grand potential can be written as [3]

$$\Omega[\rho(x,z)]=F[\rho(x,z)]+\int \rho(x,z)[v(x,z)-\mu]dx\,dy\,dz, \quad (3)$$

where $\rho(x,z)$ is the singlet number density, $F[\rho(x,z)]$ is the Helmholtz free energy, and μ is the chemical potential. The Helmholtz free-energy functional is broken into an ideal and an excess part

$$F[\rho(x,z)]=F_{\rm id}[\rho(x,z)]+F_{\rm ex}[\rho(x,z)]. \quad (4)$$

The ideal part is known exactly,

$$F_{\rm id}[\rho(x,z)]=kT\int d\mathbf{r}[\rho(x,z)[\ln \Lambda^3\rho(x,z)-1], \quad (5)$$

where Λ is the usual de Broglie wavelength. The excess free energy is obtained using the weighted density approximation [22]

$$F_{\rm ex}[\rho(x,z)]=\int \rho(x,z)f_{\rm ex}[\widetilde{\rho}(x,z)]d\mathbf{r}. \quad (6)$$

In the above $f_{\rm ex}$ is the excess (over ideal gas) free energy per particle and the weighted density $\rho(x,z)$ is given by

$$\widetilde{\rho}(x,z)=\int \rho(z',y')W(|\mathbf{r}-\mathbf{r}'|)d\mathbf{r}', \quad (7)$$

with $W(r)$ being the Tarazona weighting function given in Ref. [23].

At equilibrium, $\delta\Omega[\rho(x,z)]/\delta\rho(x,z)=0$; thus we obtain
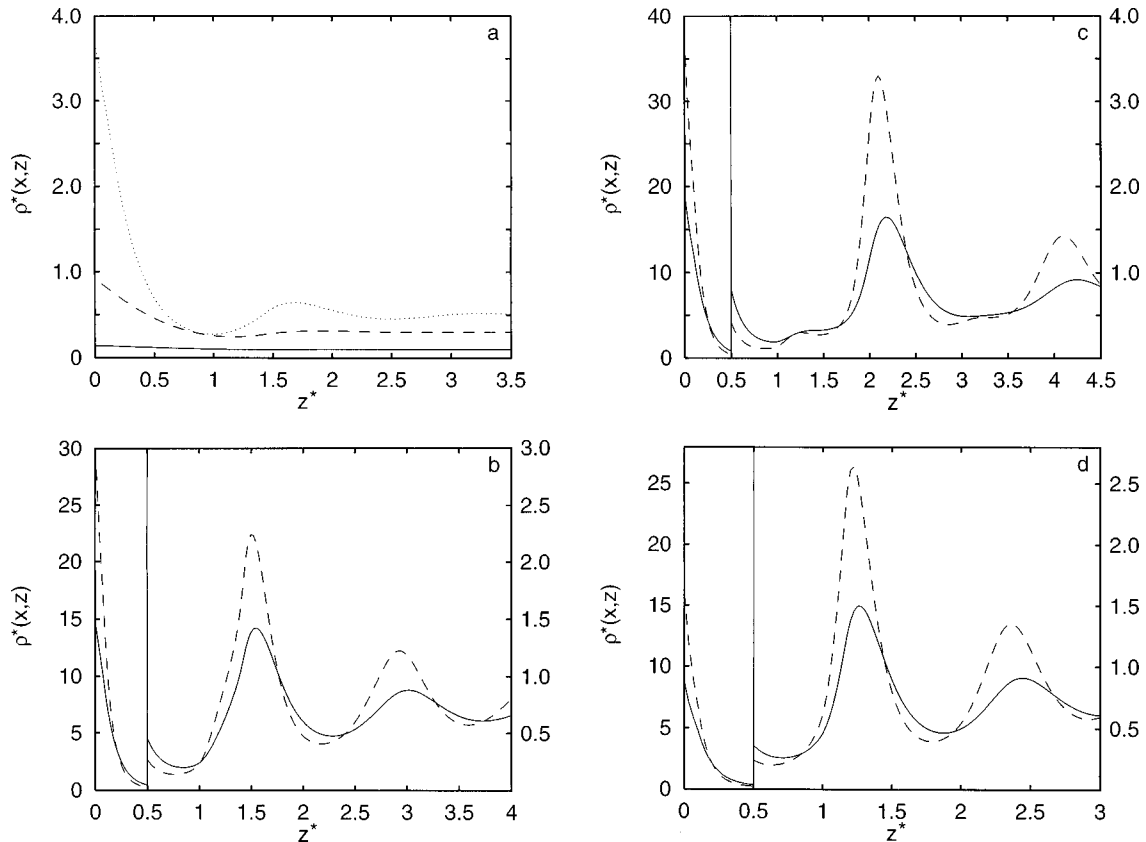
FIG. 3. Dependence of the cuts through the density distribution $\rho(x,z)$ by the plane $x=0$ on the distance z for (a) and (b) $\gamma=\pi/2$, (c) $\gamma=\pi/3$, and (d) $\gamma=2\pi/6$. There are two panels in (b) and (c) with the corresponding left- and right-hand side descriptions of the local density axis. The curves from bottom to top in (a) have been calculated at $\rho_b=0.1$, 0.3, and 0.5, respectively. In (b)–(d) the solid lines are at $\rho_b=0.7$, whereas the dashed lines are at $\rho_b=0.8$.

$$\rho(x,z) = \exp\{-[kT \ln \rho_b \mu_{\mathrm{ex}} - v(x,z) - \Phi(x,z)]/kT\}, \tag{8}$$

where ρ_b is the density of a bulk (reference) fluid that is in equilibrium with the confined fluid, μ_{ex} is its excess chemical potential, and

$$\Phi(x,z) = f_{\mathrm{ex}}[\widetilde{\rho}(x,z)]$$

$$+ \int \frac{\delta\widetilde{\rho}(x',z')}{\delta\rho(x,z)} \rho(x',z') f'_{\mathrm{ex}}[\widetilde{\rho}(x',z')] d\mathbf{r}'. \tag{9}$$

In the above f'_{ex} is the derivative of f_{ex} with respect to the density.

If the Carnahan-Starling equation of state [24] is used, then

$$f_{\mathrm{ex}}(\rho) = 2/(1-\eta) + 1/(1-\eta)^2 - 3 \tag{10}$$

and

$$\mu_{\mathrm{ex}} = \frac{4\eta - 3\eta^2}{(1-\eta)^2} + \frac{1+\eta+\eta^2-\eta^3}{(1-\eta)^3}, \tag{11}$$

where $\eta = \pi\sigma^3\rho/6$ is the packing fraction. Of course, expressions (10) and (11) can be simplified. However, it was convenient to use this form in our computer program.

The method of solution of the density profile equation (8) was based upon a standard iterational procedure. In the majority of the calculations that we performed, we used a mesh size of 0.025σ along each axis; also some of the calculations were made with a smaller grid size equal to 0.02σ. The system size is the same as in the work of Schoen and Dietrich [21], namely, $s_z = 12\sigma$ and $s' = \sqrt{s_x^2 + s_z^2} = 10\sigma$ (for the meaning of the symbols see Fig. 1). All the calculations have been carried out on the BYU Silicon Graphics Power Challenge computer with eight processors.

III. RESULTS AND DISCUSSION

To check the reliability of the computational scheme that has been used we have calculated the density profile for the system with $\gamma = \pi$, i.e., for a flat wall. The density profiles have been compared with both the Monte Carlo data of Schoen and Dietrich [21] at $\rho_b^* = \rho_b\sigma^3 = 0.7016$ and the results of the corresponding one-dimensional density-functional program. To save space we do not show these plots here, but only note that the density profile evaluated by us agrees rather well with the one given in Ref. [21] their Fig. 2, although the height of the first maximum is slightly overestimated (we obtained 4.298, whereas the simulated value is 3.972 [21]).

Figure 2 compares the cut by the plane $x^* = x/\sigma = 0.36$ through the local densities evaluated from the present theory and from the GCEMC simulation for the system with $\gamma = \pi/2$ at $\rho_b^* = 0.7016$. The agreement between the theoretical and simulational data is good.

Examples of the local densities $\rho(x=0,z)$, evaluated at different bulk densities and for the systems with different angles $\gamma = \pi/3$, $\pi/2$, and $2\pi/3$, are displayed in Fig. 3. Similarly to the case of the GCEMC simulations, a decrease of
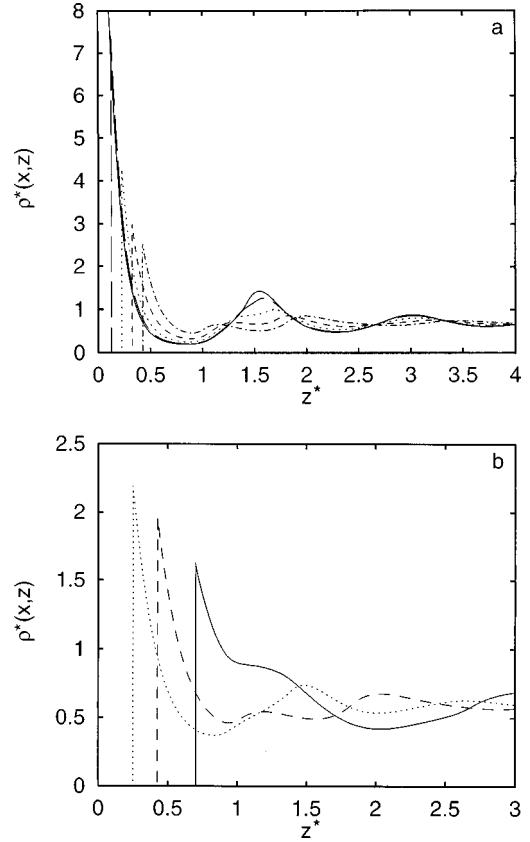
FIG. 4. Curves from left to right are the cuts of the density profile for $\gamma = \pi/2$ and $\rho_b^* = 0.7$ by the planes $x=0$, 0.1σ, 0.2σ, 0.3σ, and 0.4σ, respectively. (b) Cuts of the density profiles for $\gamma = 2\pi/3$ (dotted line), $\pi/2$ (dashed line), and $\pi/3$ (solid line) by the plane $x = 0.4\sigma$. The bulk density is $\rho_b^* = 0.6$.

the dihedral angle γ causes a substantial increase of the local density at contact. Indeed, at $\rho_b^* = 0.7$ we have $\rho^*(x=0,z=0) = \rho(x=0,z=0)\sigma^3 = 7.06$ for $\gamma = 2\pi/3$ and $\rho^*(x=0,z=0) = 19.04$ for $\gamma = \pi/3$. This behavior is not suprising. The two walls forming the wedge squeeze the hard spheres into the corner and, obviously, this effect is more pronounced for smaller values of γ. The simulation contact density obtained from the GCEMC simulations of Schoen and Dietrich for $\gamma = \pi/2$ and at $\rho_b^* = 0.7016$ is 14.34. Our result for the same point is 14.42, which is only slightly higher. Thus the agreement of the simulation and theoretical results is excellent, much better than we expected at the beginning of this study.

The distance between the first and the second density peaks depends on the angle γ. For $\gamma = \pi/2$ this distance is slightly higher than $\sqrt{2}\sigma$, which suggests that four particles form a square at the corner of the wedge, even though intuitively we would expect a more closely packed structure. For $\gamma = \pi/3$, this distance is greater than 2. Again, this suggests a looser structure than one might expect, possibly resulting from entropic effects. At the highest density there exists a small maximum in the middle of the first minimum.

Figure 4 gives further insight into the local density changes in the systems with different γ. Figure 4(a) shows the cuts by the planes $x=0$, 0.1σ, 0.2σ, 0.3σ, and 0.4σ through the density profile for $\gamma = \pi/2$ and at $\rho_b^* = 0.7$. We see here that with increasing x, the subsequent maxima are converted into minima and vice versa. Figure 4(b) illustrates
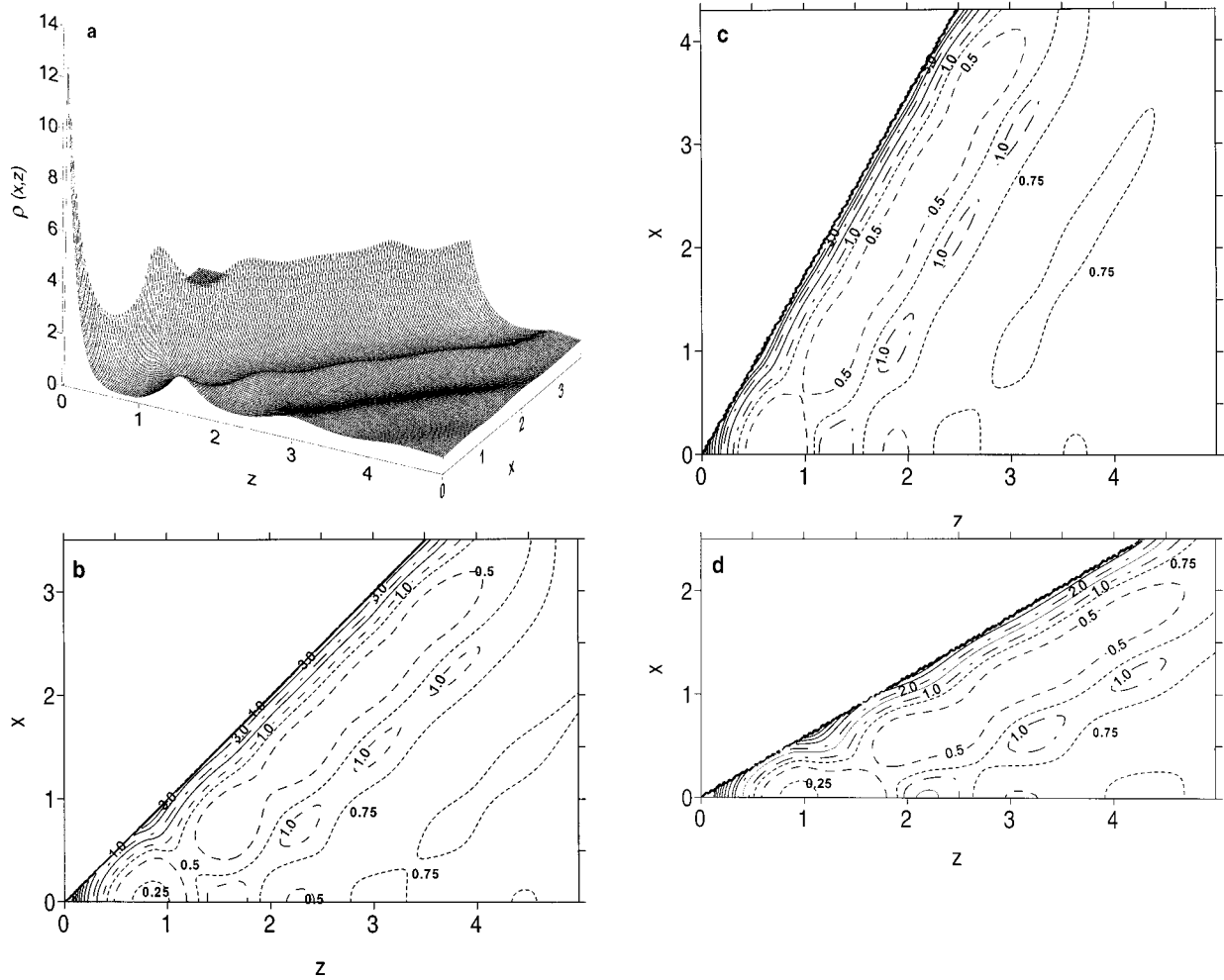
FIG. 5. (a) Three-dimensional profile $\rho(x,z)$ and (b)–(d) the contour plots for three selected dihedral angles (a) and (b) $\gamma = \pi/2$, (c) $\gamma = \pi/3$, and (d) $\gamma = 2\pi/3$. All calculations are for $\rho_b^* = 0.7$.

the variation of the cuts of the density profile by the plane $x = 0.4\sigma$ with γ and $\rho_b^* = 0.6$.

A more detailed structure of a hard-sphere fluid in a hard wedge emerges if one displays three-dimensional plots of $\rho(x,z)$ and makes contour map plots of these profiles (see Fig. 5). Comparing the contour maps for $\gamma = \pi/2$ and $2\pi/3$ [Figs. 5(b) and 5(d)] with the corresponding plots of Schoen and Dietrich, we can conclude that the structure of the fluid predicted by the density-functional approach is at least qualitatively the same as the results from the GCEMC simulations. For $\gamma = \pi/2$, a second maximum of $\rho(x,z)$ is at a distance close to $\sqrt{2}\sigma$ from the point at which the fluid is in contact with the wall along the line $x = 0$. This plot shows also that the first minimum, centered at $x = 0$, appears halfway between the point of the fluid-wall contact and the second maximum, as expected from geometrical considerations. In the x direction, the second maxima are framed by two minima [because of the symmetry, only one of them is displayed in Fig. 5(b)], separated from the first maximum by a distance approximately equal to 0.5σ.

The fluid structure evaluated for $\gamma = \pi/3$ exhibits the existence of a second maximum along the line $x = 0$ at the distance greater than 2σ from the contact fluid-corner point. This maximum is separated from the first by a widespread minimum and surrounded from both sides ($x < 0$ and $x > 0$)

by two minima. However, for $\gamma = 2\pi/3$ a typical configuration at the wedge is distinct. Two minima framing the second maximum have vanished and the contour lines are almost parallel to the solid walls.

IV. CONCLUSIONS

Most previous applications of density-functional theory to inhomogeneous fluids have been to systems with one-dimensional symmetry. In this study, we show that this approach is also successful for more complex geometries. We have obtained pleasing agreement with the recent simulations of Schoen and Dietrich. We hope to apply our multidimensional density-functional algorithm to a wide variety of inhomogeneous fluids near heterogeneous surfaces and in complex pores.

ACKNOWLEDGMENTS

[1] M. Schoen, *Computer Simulation of Condensed Phases in Complex Geometries* (Springer-Verlag, Heidelberg, 1993).

[2] M. Lozada-Cassou, in *Fundamentals of Inhomogeneous Fluids*, edited by D. Henderson (Dekker, New York, 1992), p. 303.

[3] R. Evans, in *Fundamentals of Inhomogeneous Fluids* (Ref. [2]), p. 85.

[4] D. Henderson and S. Sokołowski, Phys. Rev. E **52**, 758 (1995).

[5] W. A. Steele, *The Interaction of Gases with Solid Surfaces* (Pergamon, New York, 1974).

[6] D. Beaglehole, J. Phys. Chem. **93**, 893 (1989).

[7] S. Garoff, E. B. Sirota, S. K. Sinha, and H. B. Stanley, J. Chem. Phys. **90**, 7505 (1989).

[8] I. M. Tidswell, T. A. Rabedeau, P. S. Perhan, and S. D. Kosowsky, Phys. Rev. Lett. **66**, 2108 (1991).

[9] P. S. Pershan, Ber. Bunsenges. Phys. Chem. **98**, 372 (1994).

[10] D. Andelman, J.-F. Joanny, and M. O. Robbins, Europhys. Lett. **7**, 731 (1988).

[11] M. O. Robbins, D. Andelman, and J.-F. Joanny, Phys. Rev. A **43**, 4344 (1991).

[12] J. L. Harden and D. Andelman, Langmuir **8**, 2547 (1992).

[13] R. R. Netz and D. Andelman, Phys. Rev. E **55**, 687 (1997).

[14] M. Napiórkowski, W. Koch, and S. Dietrich, Phys. Rev. A **45**, 5760 (1992).

[15] J. E. Curry, F. Zhang, J. H. Cushman, M. Schoen, and D. J. Diestler, J. Chem. Phys. **101**, 10 824 (1994).

[16] G. Chmiel, L. Łajtar, A. Patrykiejew, and S. Sokołowski, J. Chem. Soc., Faraday Trans. **90**, 1153 (1994).

[17] E. Kozak, G. Chmiel, A. Patrykiejew, and S. Sokołowski, Phys. Lett. A **189**, 94 (1994).

[18] G. Chmiel, K. Karykowski, A. Patrykiejew, W. Rżysko, and S. Sokołowski, Mol. Phys. **81**, 691 (1994).

[19] G. Chmiel, D. Henderson, and S. Sokołowski, Polish J. Chem. **71**, 630 (1997).

[20] D. Henderson, in *Fundamentals of Inhomogeneous Fluids* (Ref. [2]), p. 177.

[21] M. Schoen and S. Dietrich, Phys. Rev. E **56**, 499 (1997).

[22] P. Tarazona, Phys. Rev. A **31**, 2672 (1985).

[23] P. Tarazona, U. M. B. Marconi, and R. Evans, Mol. Phys. **60**, 573 (1987).

[24] N. F. Carnahan and K. E. Starling, J. Chem. Phys. **51**, 635 (1989).